

Parallelization Strategies for Density Matrix Renormalization Group Algorithms on Shared-Memory Systems

G. Hager^a, E. Jeckelmann^b, H. Fehske^c and G. Wellein^a

^a*Regionales Rechenzentrum Erlangen (RRZE), Martensstraße 1, D-91058
Erlangen, Germany*

^b*Johannes-Gutenberg-Universität Mainz, Institut für Physik (Gruppe KOMET
337), Staudingerweg 7/9, D-55099 Mainz, Germany*

^c*Ernst-Moritz-Arndt-Universität Greifswald, Institut für Physik, Domstr. 10a,
D-17489 Greifswald, Germany*

Abstract

Shared-memory parallelization (SMP) strategies for density matrix renormalization group (DMRG) algorithms enable the treatment of complex systems in solid state physics. We present two different approaches by which parallelization of the standard DMRG algorithm can be accomplished in an efficient way. The methods are illustrated with DMRG calculations of the two-dimensional Hubbard model and the one-dimensional Holstein-Hubbard model on contemporary SMP architectures. The parallelized code shows good scalability up to at least eight processors and allows us to solve problems which exceed the capability of sequential DMRG calculations.

1 Introduction

During the past decade the density matrix renormalization group (DMRG) [1,2] has been established as a powerful numerical technique for solving many-body problems in Interacting Electron Systems, Classical Statistical Physics, and Quantum Chemistry (for a review, see [3]). For strongly correlated quantum lattice systems, DMRG techniques complement and sometimes even replace traditional methods like exact diagonalization (ED) or (Quantum) Monte Carlo algorithms [4]. In particular, for quantum systems in one spatial dimension and short-range interactions DMRG provides approximations to the ground state, to the low-lying excited states and to spectral properties with high accuracy at a modest computational effort.

Although the computational requirements can easily exceed the resources of sequential computers such as PCs or workstations and grow rapidly with increasing complexity (dimensionality or range of interactions), no efficient parallelization approach has been introduced for DMRG algorithms to date. Starting from a sequential C++ package developed by White and Jeckelmann we discuss two shared-memory parallelization strategies for the superblock diagonalization and analyze their scalability and performance on state of the art SMP systems like IBM p690, SGI Origin and Intel Itanium2-based servers.

The first approach uses the inherent parallelism contained in the dominating operation of all DMRG calculations, i.e. dense matrix-matrix multiplication (generally implemented as a call to the BLAS subroutine DGEMM). This is the lowest possible parallelization level and is thus prone to scale badly, especially in certain numerical limits where the matrices tend to be small and the parallelization overhead becomes dominant. It is nevertheless a viable strategy when the numerical structure of the problem at hand is appropriate. In those rare cases, a significant percentage of theoretical peak performance can be achieved.

The second approach targets the parallelization of the sparse matrix-vector multiplication contained in the superblock diagonalization algorithm and overcomes the overhead-induced performance bottlenecks of parallel DGEMM. Here we use OpenMP to achieve better scalability at the cost of an only slightly more complicated code structure. DMRG calculations can then be carried out with sufficient parallel efficiency on up to eight CPUs, depending on the physical problem. Modern supercomputer architectures of the SMP cluster type with large-memory SMP nodes comprising up to eight or sixteen CPUs are the primary target systems on which this approach can be used with success.

In the following section we will very briefly discuss the basics of the DMRG algorithm and its implementation in the software package used as a starting point for parallelization. Section 3 deals with the two different parallelization strategies and gives some estimates about expected performance. In section 4 we will present the results of performance measurements on different architectures. Section 5 then illustrates the benefits of parallel DMRG, introducing some physical results not obtainable with ED methods. Finally, section 6 gives some conclusions and summarizes what has yet to be done.

2 DMRG Algorithm

2.1 Basics

Determining the ground state and spectral properties of interacting quantum lattice models like e. g. the Hubbard model

$$H_{\text{HM}} = -t \sum_{\langle ij \rangle, \sigma} [c_{i\sigma}^\dagger c_{j\sigma} + \text{H.c.}] + U \sum_i n_{i\uparrow} n_{i\downarrow} \quad , \quad (1)$$

or the Holstein-Hubbard model

$$H_{\text{HHM}} = H_{\text{HM}} + g\omega_0 \sum_{i,\sigma} (b_i^\dagger + b_i) n_{i\sigma} + \omega_0 \sum_i b_i^\dagger b_i \quad (2)$$

is a fundamental but difficult problem in solid-state physics. Here, $c_{i\sigma}^\dagger$ ($c_{i\sigma}$) denote fermionic creation (annihilation) operators of spin- σ ($\sigma \in \{\uparrow, \downarrow\}$) electrons, $n_{i\sigma} = c_{i\sigma}^\dagger c_{i\sigma}$, and b_i^\dagger (b_i) are the corresponding bosonic phonon creation (destruction) operators (for the construction of the Hilbert space basis see, e. g., Ref. [5]).

The Hubbard model, independently proposed in 1963 by Gutzwiller, Hubbard and Kanamori [6], was originally designed to describe the ferromagnetism of transition metals. The physics of the model is governed by the competition between electron itinerancy (t ; delocalization) and short-range Coulomb repulsion (U ; localization, magnetic order), where the fermionic nature of the charge carriers is of great importance (Pauli exclusion principle, i.e., the existence of an ‘effective’ long-range interaction). Besides the ratio U/t , the particle density n , the temperature T , and the spatial dimension D (geometry of the lattice) are crucial parameters involved in the model. Successively, the Hubbard model was studied in the context of magnetism, metal-insulator (Mott) transition, heavy fermions and high-temperature superconductivity as the probably most simple model to account for strong correlation effects.

In addition to the purely electronic interactions in the Hubbard model it is often necessary to incorporate the coupling to lattice degrees of freedom to describe the electronic properties of solids. In the Holstein-Hubbard model [7], the second term couples the electronic system locally to an internal optical degree of freedom of the effective lattice, whereas the third term takes into account the elastic energy of a harmonic lattice. g and ω_0 denote the electron-phonon coupling constant and the phonon frequency, respectively. In the single-electron case, the Holstein model has been studied extensively as a paradigmatic model for polaron formation. At half-filling the electron-phonon

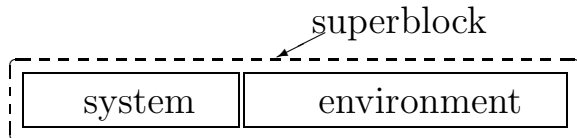


Fig. 1. *Division of the complete physical system into “system block” and “environment block”. Both blocks together form the “superblock” whose Hamiltonian matrix is diagonalized.*

coupling may lead to a Peierls instability (in competition to the antiferromagnetic instability triggered by U).

Although a tremendous amount of work has been devoted to the solution of the Hubbard and Holstein-Hubbard models, exact results are very rare and only a few special cases and limits have so far been understood analytically. Therefore a numerical treatment of both models seems to be inevitable.

Due to the locality of interactions, the matrix representation of the Hamiltonian operator H in a real-space basis is generally very sparse. In an ED approach this matrix is (partially) diagonalized with Lanczos, Davidson or similar algorithms. The dominant operation is then a sparse matrix-vector multiplication (MVM) of H with some vector \vec{v} . Due to the exponential growth of degrees of freedom with increasing system size, ED methods are limited to relatively small systems and generally require vast computing resources and memory bandwidth.

The DMRG algorithm [1,2,8] tries to overcome those drawbacks by implementing a variational scheme that truncates the Hilbert space used to represent H in an optimal way. It is the selection of the basis states that lays the groundwork on which DMRG is built.

2.2 The Algorithm

DMRG splits the physical system (usually in real space, although a momentum space approach is possible) into two pieces, the so-called *system block* and the *environment block*. Both together form the *superblock* (see Fig. 1).

The central entity in the algorithm is the *reduced density matrix*

$$\rho_{ii'} = \sum_j \psi_{ij}^* \psi_{i'j} \quad , \quad (3)$$

where i and j label the states of the system and environment blocks, respec-

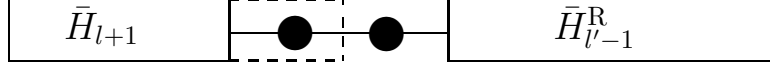


Fig. 2. One step of the finite system DMRG algorithm (left-to-right phase). \bar{H}_{l+1} and \bar{H}_{l-1}^R are system block and environment block Hamiltonians in the reduced density matrix eigenbasis.

tively, so that a superblock state $|\psi\rangle$ can be composed:

$$|\psi\rangle = \sum_{ij} \psi_{ij} |i\rangle |j\rangle . \quad (4)$$

Definition (3) shows that in ρ the states of the environment block are summed over. In this manner all possible boundary conditions that the environment may impose on the system are incorporated in the density matrix. It can now be shown [8] that the eigenstates of ρ with the largest eigenvalues are those that have the most significant impact on observables, i. e. in order to get a good guess at an optimal basis set for the superblock Hamiltonian one has to

- diagonalize the reduced density matrix for a system block of size l and extract the m eigenvectors with largest eigenvalue,
- construct all relevant operators (system block and environment Hamiltonians, observables) for a system block of size $l + 1$ in the reduced density matrix eigenbasis,
- form a superblock Hamiltonian from the system and environment block (size $l - 1$) Hamiltonians plus two single sites (see Fig. 2) and determine its ground state by diagonalization.

These steps must be repeated several times, shifting the interface between system block and environment block back and forth until some convergence criterion is fulfilled. This might be e. g. stationarity of the ground state energy or a sufficiently small *discarded weight*, which is the sum of all density matrix eigenvalues that were not considered when forming the basis. The procedure can be generalized to two dimensions, although it is not quite clear as to how the best “path” for the sweeps through the grid should be chosen [8].

The accuracy of observables like the ground state energy depends on the number m of density matrix states kept. The discarded weight gives some hint for choosing the right m for a particular problem. Usually one starts with m rather small and increases m every time the ground state energy has converged. Nevertheless most of the computing time is spent in the sweeps with largest m . Sensible values for m depend on the physical model under consideration. In the one-dimensional case where DMRG usually performs best, $m = 500$ to 1000 is often sufficient to get decent data, even for models with electron-phonon interaction like the HHM (2). In two dimensions a larger m is in order, e. g. $m = 2000$ to 10000 for a 2D Hubbard model (1). Although in

that case performance and memory requirements easily exceed the resources of standard PCs, they are still far below those needed for an ED approach, and valuable results can often be obtained on off-the-shelf hardware instead of teraflop-class supercomputers (see section 4).

It must be stressed that many complications show up in implementing the algorithm for a real-world problem. Fermionic and bosonic commutation rules, reflection and other symmetries, boundary conditions, degeneracies etc. all require special attention [4,2]. Here we wish to concentrate on the performance and parallelization aspects alone.

Diagonalization of the superblock Hamiltonian is the most time-consuming part of the algorithm and is usually done by a Lanczos or Davidson procedure. Thus repeated multiplications of H with superblock vectors ψ have to be performed. This is not done by constructing H explicitly as a matrix, but by using the fact that a Hamiltonian that describes the concatenation of two blocks can be written as

$$H_{ij;i'j'} = \sum_{\alpha} A_{ii'}^{\alpha} B_{jj'}^{\alpha} \quad , \quad (5)$$

where A and B are operators in the two blocks and α counts different terms in the Hamiltonian. Due to the fact that H “lives” in two blocks and thus has double indices, the MVM is actually of the matrix-matrix type at the lowest level:

$$\sum_{i'j'} H_{ij;i'j'} \psi_{i'j'} = \sum_{\alpha} \sum_{i'} A_{ii'}^{\alpha} \sum_{j'} B_{jj'}^{\alpha} \psi_{i'j'} \quad . \quad (6)$$

Dense matrix-matrix multiplication can be optimized using standard unrolling and blocking techniques [9] so that peak performance is theoretically achievable on modern cache-based RISC architectures. This is not quite true for very small matrices, where loop overhead and pipeline fill-up effects come into play, but the MVM part of DMRG is nevertheless well suited for RISC machines.

A slight complication arises because it is quite unfavourable with respect to performance and memory requirements to use dense matrices throughout. Many operators only have nonzero matrix elements between states with specific quantum numbers (or quantum number differences), so that it is sufficient to store the nonzero blocks. Those blocks are labeled by indices $R(k)$ on the RHS and are, by virtue of the MVM, mapped to blocks with indices $L(k)$ on the LHS. Consequently, there is an additional sum over quantum numbers in (6). Omitting the “normal” matrix indices, (6) becomes

$$H\psi = \sum_{\alpha} \sum_k (H\psi)_{L(k)}^{\alpha} = \sum_{\alpha} \sum_k A_k^{\alpha} \psi_{R(k)} [B^T]_k^{\alpha} \quad . \quad (7)$$

In the software package developed by White and Jeckelmann, the structure of MVM in the Davidson algorithm is exactly as shown above, featuring two nested loops that handle Hamiltonian terms and quantum numbers separately.

Every shared-memory parallelization attempt must identify loops in the algorithm that lend themselves to parallel execution. In (7) three such loops are visible: the innermost matrix-matrix multiplication (twice), the sum over quantum numbers and the sum over terms in the Hamiltonian.

3 Parallelization of the Superblock Diagonalization

As shown in the previous section, the performance of (non-dynamical) DMRG calculations is governed by the superblock diagonalization algorithm, in which a sparse MVM plays the dominant role. Fortunately the basic operation in this sparse MVM is dense matrix-matrix multiplication, which is well optimized in the form of BLAS DGEMM on most architectures. Single-CPU performance of DMRG calculations can potentially achieve a significant fraction of peak speed.

SMP parallelization can be performed in a variety of ways, two of which are targeted here: DGEMM threading and OpenMP in the sparse MVM procedure.

3.1 *Shared-Memory DGEMM parallelization*

This approach is the simplest one possible due to the fact that no additional programming effort is necessary. Parallel BLAS libraries exist for virtually all contemporary SMP architectures, thus relinking with another library is all that is required. All parallelization complexities are hidden inside vendor-provided DGEMM code.

Unfortunately, the DMRG method has an important drawback — the matrices which form the operands for DGEMM calls are often quite small, leading to non-negligible parallelization overhead (load imbalance, barrier wait, thread wakeup). This fact makes the DGEMM approach unsuitable for a large class of problems. See section 4 for performance results.

3.2 *OpenMP Parallelization of MVM*

One of the basic rules of OpenMP parallelization is to try to find loops that are as far as possible at the outside of a loop nest and identify their parallelism.

The sparse MVM at the core of the Davidson diagonalization routine is a viable target for this approach.

In a first attempt one would simply use an `omp parallel for` directive at the outer loop of (7). This, however, yields unsatisfactory performance because the outer loop goes over the terms in the Hamiltonian, and although the number of terms can easily become a couple of hundreds (especially when using a large number of sites), load imbalance will readily show up. Moreover the number of terms can become very small in the course of the calculation when the system block comprises a couple of sites only.

The inner loop over the quantum numbers suffers essentially from the same deficiencies when it comes to parallelization. In order to get proper scaling, the loop nest has to be eliminated, leading to a single loop. This is the original code of the loop nest:¹

```
1 // W is wave vector, R ist result
2 for(i=0; i < number_of_hamiltonian_terms; i++)
3   {
4     term = hamiltonian_terms[i];
5     for(q=0; q < term.number_of_blocks; q++)
6       {
7         li = term[q].left_index;
8         ri = term[q].right_index;
9
10        temp_matrix = term[q].B.transpose() * W[ri];
11        R[li] += term[q].A * temp_matrix;
12      }
13   }
```

The outer loop is for the Hamiltonian terms whereas the inner loop counts quantum numbers. The `StateSet` indices `li` and `ri` identify blocks with certain quantum numbers in the wave vectors. There are some peculiarities one must take care of:

- Every loop iteration writes to some part of the result vector, identified by `li`. Parallelization must account for the possibility that any two iterations might have the same value for `li`.
- The trip count for the inner loop is not a constant but depends on the term.

So when replacing the loop nest by a single loop, one has to take some measures with respect to bookkeeping. First, a prologue loop must prepare an array that stores references to all blocks required:

¹ The pseudocode snippets in this section are simplified excerpts that serve to illustrate the coding strategy. They do not constitute runnable code.


```

1 for (ics=0,i=0; i < number_of_hamiltonian_terms; i++)
2   {
3     term = hamiltonian_terms[i];
4     for(q=0; q < term.number_of_blocks; q++)
5       {
6         block_array[ics] = &term[q];
7         ics++;
8       }
9   }
10  icsmax = ics;

```

Second, an array of OpenMP locks has to be set up (once) that later protect from race conditions when updating the result vector. This array could potentially be established using a C++ vector class (dynamic resizeability), but experience shows that most compilers have severe difficulties in parallelizing OpenMP loops that handle complicated C++ objects. Thus the necessary arrays were declared as having a fixed length, and appropriate checking mechanisms (not shown here) prevent boundary violation:

```

1 static int flag=0;
2 if(!flag)
3   {
4     flag=1;
5     for(i=0; i < MAX_NUMBER_OF_THREADS; i++)
6       mm[i] = new Matrix // temp. matrix
7     for(i=0; i < MAX_NUMBER_OF_LOCKS; i++)
8       {
9         locks[i] = new omp_lock_t;
10        omp_init_lock(locks[i]);
11      }
12  }

```

Now the loop nest can be transformed into a single parallel loop. The required temporary matrix for each thread is provided inside the parallel region but before the loop actually starts:

```

1 #pragma omp parallel private(mytmat,li,ri,myid,ics)
2   {
3     myid = omp_get_thread_num();
4     mytmat = mm[myid]; // temporary matrix, thread-local
5 #pragma omp for
6   for(ics=0; ics < icsmax; ics++)
7     {
8       li = block_array[ics]->left_index; // StateSet indices
9       ri = block_array[ics]->right_index;
10
11

```

```

12     mytmat = block_array[ics]->B.transpose() * W[ri];
13
14     omp_set_lock(locks[li]);
15     R[li] += block_array[ics]->A * mytmat;
16     omp_unset_lock(locks[li]);
17 }

```

Only the second matrix-matrix multiplication has to be protected via OpenMP locks, as it writes to block number `li` of the result vector. The first one stores its result in a thread-local temporary matrix.

In our default benchmark case (see following section), sparse MVM takes about 85 % of total computing time in the serial case. We therefore expect parallel speedups of up to 6 or 7, not taking into account mutual locking overhead, thread startup and the like.

4 Performance Results on Contemporary SMP Systems

Two benchmark cases have been investigated in order to show the performance of the different parallelization strategies:

- (1) The ‘default’ benchmark case used here, unless otherwise noted, is a calculation of ground state properties for the Hubbard Model (1) in two dimensions with 4x4 sites and periodic boundary conditions (BCs) at half-filling with $U = 4$ and isotropic delocalization $t_{x,y} = 1$. Although we stick to $m = 2000$ for practical reasons, the number of density matrix states kept, m , must be larger ($m \approx 7000$) to obtain a good approximation of the ground state wavefunction, in particular, to preserve translational invariance.
- (2) The second benchmark, an 8-site one-dimensional Holstein-Hubbard system (2) at $U = 3$, $t = 1$, $\omega_0 = 1$, $g^2 = 2$ and periodic BCs, has been chosen to show the deficiencies of the parallelization approach. We represent each boson site with six pseudosites [4] corresponding to a maximum of 64 phonons per boson site. Thus, the effective number of DMRG sites is 56. To achieve convergence $m = 900$ has to be used.

Although this study deals mainly with scalability, we nevertheless specify one-CPU performance numbers for all systems under investigation in order to set the scale (Table 1). Although it is clear that performance is always dominated by the Davidson diagonalization, the quality of the C++ compiler and the DGEMM implementation have some influence, the latter especially due to the abundance of small and non-square matrices. Because of a sophisticated, object-oriented data housekeeping structure in the code, proper inlining and

Table 1

One-CPU performance in GFlop/s and efficiency in terms of fraction of peak performance for all systems studied (benchmark case 1). Proprietary, vendor-supplied BLAS and LAPACK implementations were used in all cases.

System	Peak Perf. [GFlop/s]	DMRG Perf. [GFlop/s]	Fraction of Peak
IBM p690/Power4 (1.3 GHz)	5.2	2.78	0.53
HP rx5670/Itanium2 (1 GHz)	4.0	2.25	0.56
Intel Xeon DP (2.4 GHz)	4.8	2.08	0.43
SunFire 3800 (900 MHz)	1.8	0.92	0.51
SGI Origin 3400 (500 MHz)	1.0	0.78	0.78

optimization is essential as well. A comparison with peak performance for every system (last column in Table 1) shows deficiencies in those respects quite prominently.

For parallel performance studies there are essentially two metrics that can be considered: Speedup $S(N)$ and parallel efficiency $\varepsilon(N)$. If $P(N)$ is the performance of the benchmark on N processors, then

$$S(N) = \frac{P(N)}{P(1)} \quad \text{and} \quad \varepsilon(N) = \frac{S(N)}{N} . \quad (8)$$

In the following we will present data for one or the other metric as appropriate.

An important limitation to parallel efficiency and speedup is imposed by a theoretical limit called *Amdahl's Law*. In a simple model one can split a single-threaded application into a serial (non-parallelizable) fraction s and a perfectly parallelizable fraction $p = 1 - s$. The speedup with N CPUs is then calculated as

$$S_A(N) = \frac{s + p}{s + \frac{p}{N}} = \frac{1}{s + \frac{1-s}{N}} , \quad (9)$$

with

$$\lim_{N \rightarrow \infty} S_A(N) = \frac{1}{s} . \quad (10)$$

In our case the serial fraction is strongly influenced by the quality of the C++ compiler, which has thus a large impact on scalability. As already mentioned in section 3.2, the typical fraction of 85% of the total computing time for the sparse MVM (leading to $p = 0.85$ in the Amdahl model) leads to the

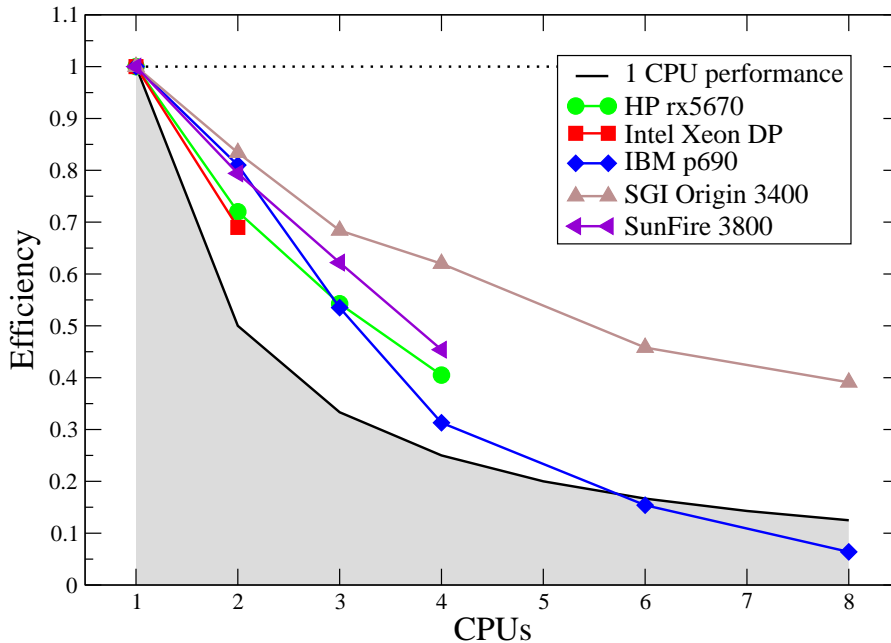


Fig. 3. Parallel efficiency on different SMP systems (whole program) with DGEMM parallelization, benchmark case 1. The grey region marks the limit where no speedup is gained compared to the 1-CPU run.

expectation that speedups between 6 and 7 are achievable when parallelization overhead is negligible.

4.1 Parallel DGEMM

Using parallel DGEMM is as easy as relinking with the appropriate library on all systems, and is available everywhere. Parallel efficiency was measured on a variety of architectures (see Fig. 3). As can be seen from the parallel efficiency data, this is actually a very poor method for parallelization. Scalability depends heavily on the quality of the implementation of parallel DGEMM, as well as more obscure features like hardware barriers and associated loss. Compared to other systems, the SGI Origin still does quite well, which can at least partly be attributed to the high-quality C++ compiler.

Fig. 3 also shows the limit where parallelization becomes entirely useless (grey zone), i. e. where N -CPU performance drops below the 1-CPU case.

4.2 OpenMP Parallelization

The OpenMP variant of the program unfortunately runs only with SGI and IBM systems. Intel and Sun compilers have deficiencies that either prevent

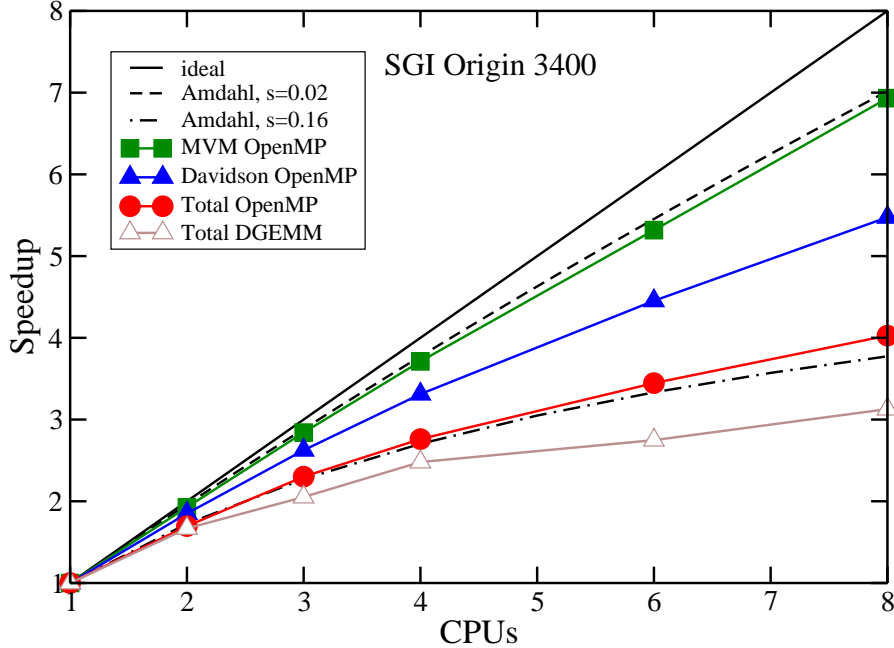


Fig. 4. *OpenMP scaling on SGI Origin 3400, benchmark case 1. Scaling of whole program, Davidson algorithm and MVM are shown separately, as well as Amdahl scaling for serial fractions $s = 0.05$ and $s = 0.16$.*

the code from compiling or generate nonfunctional programs.

Fig. 4 shows the results of a scaling run with up to 8 CPUs on an Origin 3400 system, where scaling is broken down to different abstraction levels (MVM, Davidson, whole program). While the “whole program” scaling is what the end user is finally interested in, it is quite clear that some significant optimization potential is still hidden between Davidson diagonalization and sparse MVM. Amdahl scaling for two different serial fractions ($s = 0.02$ and $s = 0.16$) is also shown. Although the Amdahl performance model is admittedly too simplistic for this code, it nevertheless gives a rough impression about what has been achieved. Obviously, the MVM parallelization is very efficient with only a minor serial fraction.

Fig. 5 displays the parallel efficiency of the code on IBM p690 and SGI Origin 3400 systems. In contrast to the DGEMM parallelization case, SGI does not have an advantage here. Although the two systems are practically on par with respect to scalability, a direct comparison of performance in GFlop/s shows clearly what the favourable architecture for DMRG today should be (Fig. 6).

As the Davidson procedure itself is very well parallelizable, we expect that some performance boost is still in reach. Other aspects of the implementation that become more prominent with other physical setups also bear some optimization potential. An example for this is the Holstein-Hubbard model (benchmark case 2) for which the broken-down parallel profiling data is shown

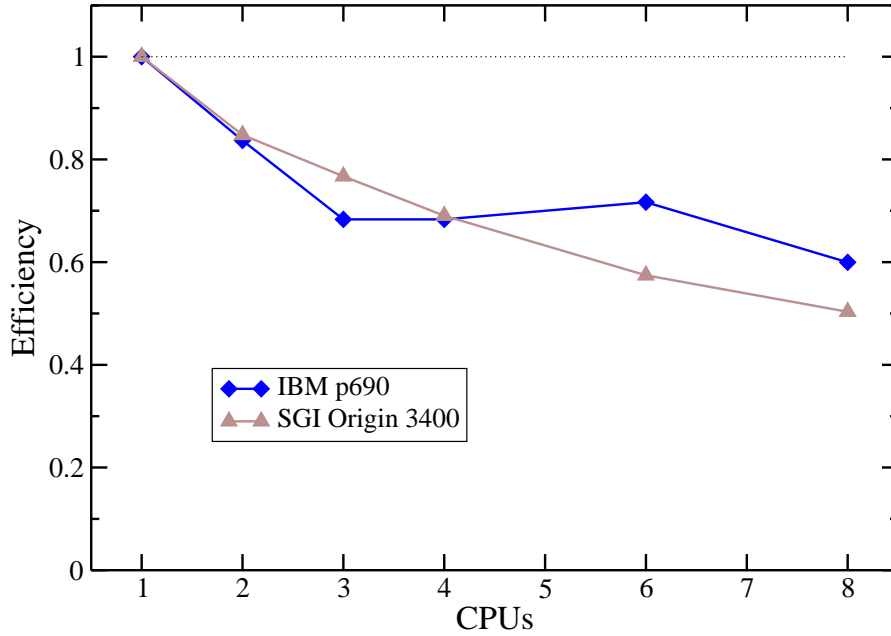


Fig. 5. *OpenMP* parallel efficiency on IBM p690 and SGI Origin SMP systems (whole program), benchmark case 1. The data for the IBM system was taken on a loaded system.

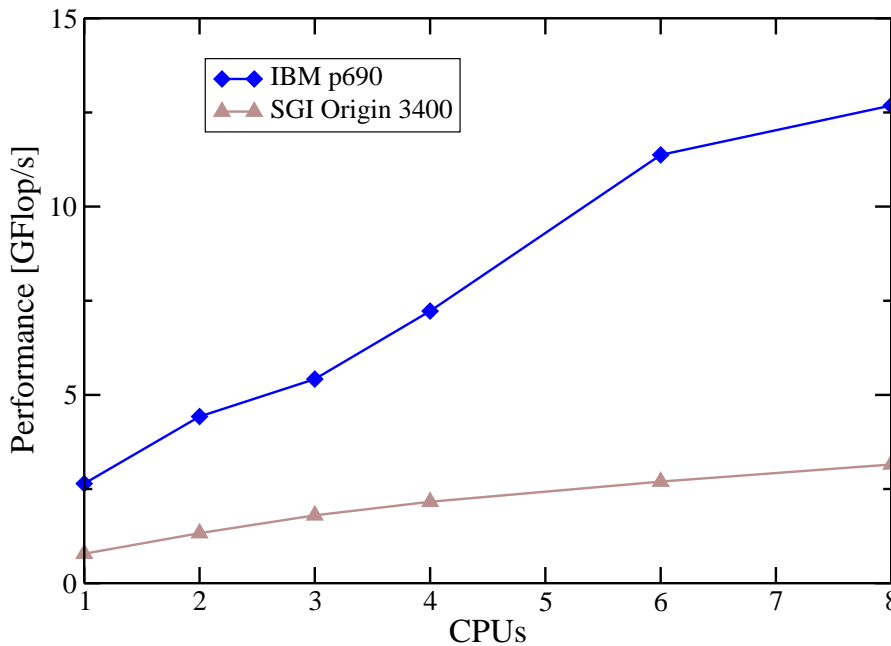


Fig. 6. *OpenMP* absolute performance in GFlop/s on IBM p690 and SGI Origin SMP systems (whole program), benchmark case 1.

in Fig. 7. Here we see that the mediocre overall speedup is actually caused by the sparse MVM itself. Profiling reveals that a significant amount of time is spent in acquiring locks for the parts of the result vector. Reordering the loop iterations may help here and is being investigated.

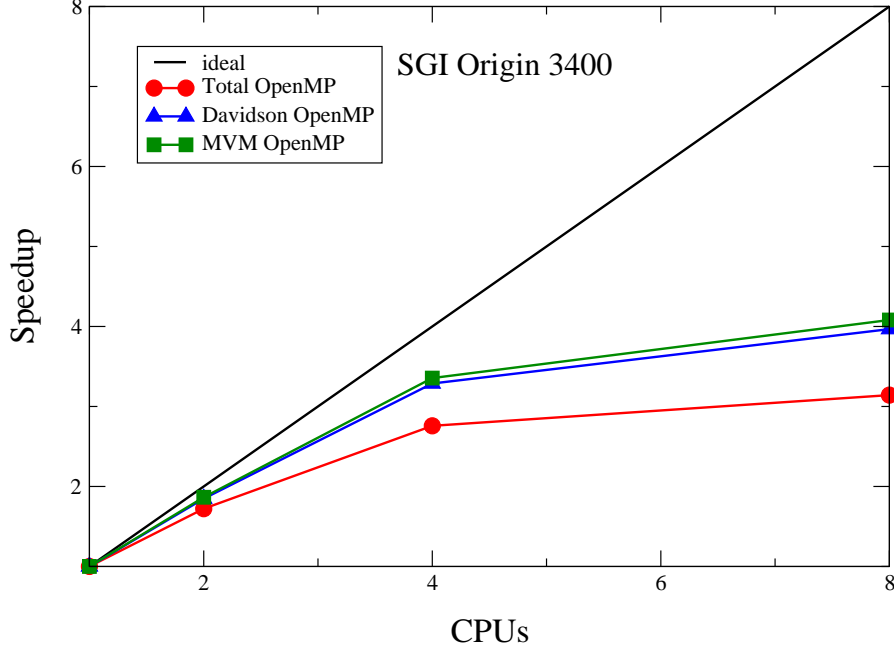


Fig. 7. *OpenMP scaling for benchmark case 2.*

5 Application: Peierls-Insulator Mott-Insulator Transition in 1D

In quasi-one-dimensional (1D) materials there is a strong competition between electron-electron and electron-phonon interactions, which tend to localize the charge carriers by establishing commensurate spin-density-wave and charge-density-wave ground states, respectively. At half-filling, in particular, Peierls (PI) or Mott (MI) insulating phases are favored over the metallic state. A heavily debated issue concerns the nature of the quantum phase transitions between the different insulating phases (for more details see [10] and references therein). The Holstein-Hubbard model is perhaps the most simple model to address this problem because it shows a PI-MI transition with increasing U above a threshold electron-phonon coupling (a critical electron-phonon coupling is required in order to establish the PI state at nonzero phonon frequency). For finite periodic chains it has been verified that the transition results from a ground state level crossing with a change in the ground state site-parity eigenvalue. As can be seen from Fig. 8, the staggered charge- and spin-structure factors,

$$S_c(\pi) = \frac{1}{N^2} \sum_{\substack{i,j \\ \sigma,\sigma'}} (-1)^{|i-j|} \langle (n_{i\sigma} - \frac{1}{2})(n_{j\sigma'} - \frac{1}{2}) \rangle , \quad (11)$$

$$S_s(\pi) = \frac{1}{N^2} \sum_{i,j} (-1)^{|i-j|} \langle S_i^z S_j^z \rangle , \quad S_i^z = \frac{1}{2}(n_{i\uparrow} - n_{i\downarrow}) , \quad (12)$$

are strongly suppressed approaching the quantum critical point from below and above, respectively. However, both $S_c(\pi)$ and $S_s(\pi)$ remain finite at the transition point for the small 8-site system we were able to study by means of ED techniques in previous work. Fig. 8 shows that good agreement between ED and DMRG is achievable for this case. Using the parallelized DMRG

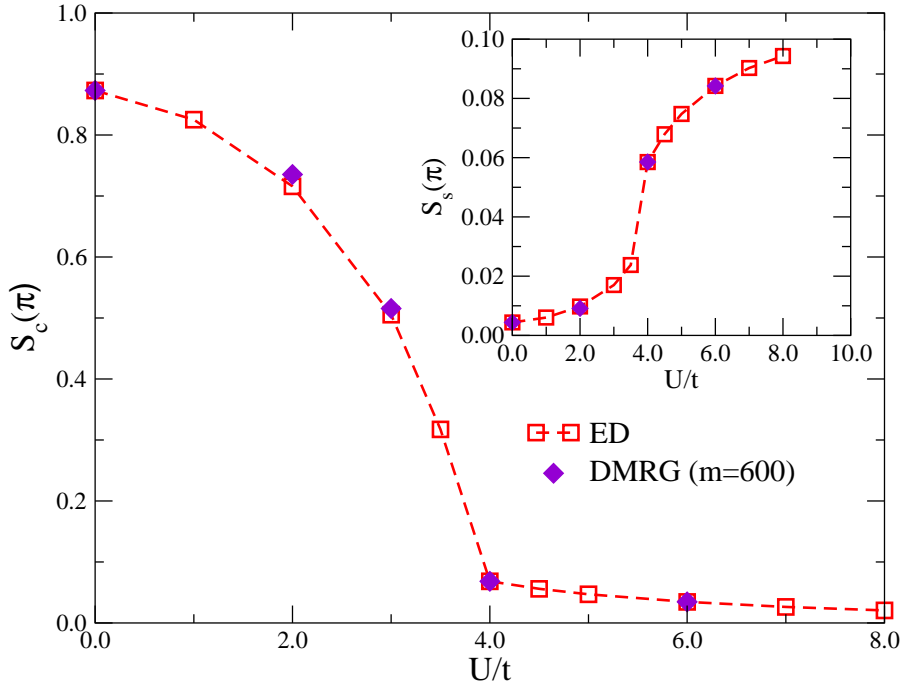


Fig. 8. Spin and charge structure factors at $q = \pi$ in the half-filled one-dimensional 8-site HHM (2) with periodic BCs for different U at $t = 1$, $\omega_0 = 1$ and $g^2 = 2$. Squares denote ED results, diamonds show DMRG calculations with $m = 600$ and six pseudosites.

code for the Holstein-Hubbard model we are now in the position to calculate spin and charge structure factors for a sequence of systems with up to 32 sites. The results presented in Fig. 9 can be used to perform a reliable finite-size extrapolation: At the quantum critical point $S_c(\pi)$ and $S_s(\pi)$ vanish in the thermodynamic limit $N \rightarrow \infty$. Simultaneously the optical excitation gap closes.

A comparison of the required resources for this problem shows already in the 8-site case quite clearly the superior capabilities of the DMRG method for this kind of problem (Table 2). For the 32-site lattice (leftmost data point in Fig. 9) with five pseudosites (32 phonons per boson site), the overall number of sites is 192. Such a system would be absolutely unmanageable with ED methods.

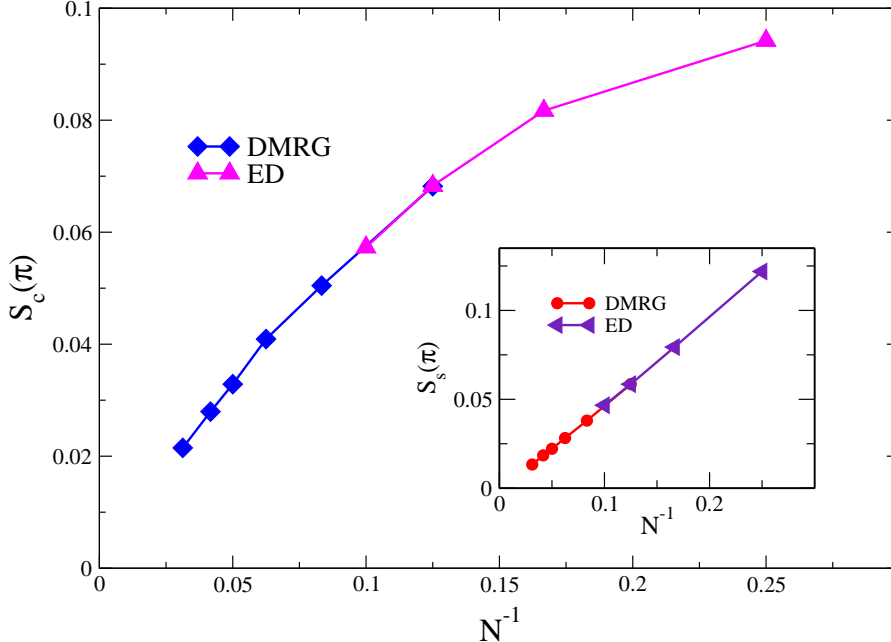


Fig. 9. *Finite-size scaling study of spin and charge structure factors at $q = \pi$ in the half-filled one-dimensional HHM (2) with periodic BCs at $U = 4$, $t = 1$, $\omega_0 = 1$ and $g^2 = 2$ with five boson pseudosites, $m = 1000$ and lattice sizes of up to 32. For reference, available ED calculations are shown as well.*

Table 2

Comparison of computational resources for the calculation of spin and charge structure factors in the Holstein-Hubbard Model

Method	# of CPUs	Walltime	Memory
ED (8 sites, matrix dim. $\sim 10^{10}$)	1024 (Hitachi SR8000)	~ 12 hrs	600 GB
DMRG (8 sites, $m = 600$)	1 (SGI Origin)	~ 18 hrs	2 GB
DMRG (24 sites, $m = 1000$)	4 (SGI Origin)	~ 72 hrs	10 GB

6 Conclusions and Outlook

We have presented two methods for parallelization of a DMRG code on shared-memory systems: parallel DGEMM and OpenMP parallelization on the Davidson MVM level. The deficiencies of parallel DGEMM are quite clear, but it is still the only alternative when one has to stick to compilers that do not support OpenMP directives (correctly). OpenMP does much better, and there is some significant parallelization potential still hidden in the code outside the MVM subroutine that must be exploited. We expect that the parallel code will scale well up to sixteen CPUs without any changes in the DMRG algorithm. A radically different parallelization approach or a new DMRG algorithm would be necessary to obtain reasonable scalability on hundreds of processors in massively parallel computers. However, the current SMP implementation already

allows us to investigate much larger systems than with ED or with sequential DMRG.

Acknowledgements

We thank the RRZE, the RZG (Computing Center Garching), the URZ (Universitätsrechenzentrum Dresden) and the HLRS (High Performance Computing Center Stuttgart) for providing computational resources. The RRZN (Regionales Rechenzentrum Niedersachsen) and the ZIB (Zuse-Institut Berlin) have granted resources on their HLRN supercomputer complex. This work was partially supported by the Bavarian Competence Network for High Performance Computing (KONWIHR).

References

- [1] S.R. White, Density Matrix Formulation for Quantum Renormalization Groups. *Phys. Rev. Lett.* **69**, 2863–2866 (1992)
- [2] S.R. White, Density-Matrix Algorithms for Quantum Renormalization Groups. *Phys. Rev. B* **48**, 10345–10356 (1993)
- [3] I. Peschel, X. Wang, M. Kaulke and K. Hallberg (eds), *Density-Matrix Renormalization: A New Numerical Method in Physics*. Springer, Berlin Heidelberg New York (1999) (Lecture Notes in Physics Vol. 528)
- [4] E. Jeckelmann and S.R. White, Density-Matrix Renormalization Group Study of the Polaron Problem in the Holstein Model. *Phys. Rev. B* **57**, 6376–6385 (1998)
- [5] G. Wellein, H. Röder, and H. Fehske, Polarons and Bipolarons in Strongly Interacting Electron-Phonon Systems. *Phys. Rev. B* **33**, 9666–9675 (1996)
- [6] M. C. Gutzwiller, Effect of Correlation on the Ferromagnetism of Transition Metals *Phys. Rev. Lett.* **10**, 159–162 (1963); J. Hubbard, Electron Correlations in Narrow Energy Bands. *Proc. Roy. Soc. London A* **276**, 238–257 (1963); J. Kanamori, Electron Correlation and Ferromagnetism of Transition Metals, *Prog. Theor. Phys.* **30**, 275–289 (1963)
- [7] T. Holstein, Studies of Polaron Motion. 1. The Molecular Crystal Model. *Ann. Phys. (N.Y.)* **8**, 325–342 (1959); Studies of Polaron Motion. 1. The Small Polaron. *Ann. Phys. (N.Y.)* **8**, 343–389 (1959)
- [8] R.M. Noack and S.R. White, The Density Matrix Renormalization Group. In: I. Peschel, X. Wang, M. Kaulke and K. Hallberg (eds), *Density-Matrix Renormalization: A New Numerical Method in Physics*. Lectures of a seminar

and workshop, held at the Max-Planck-Institut für Physik Komplexer Systeme, Dresden, Germany, August 24th to September 18th, 1998. Springer, Berlin Heidelberg New York (1999) (Lecture Notes in Physics Vol. 528)

- [9] S. Goedecker and A. Hoisie, Performance Optimization of Numerically Intensive Codes. Siam, Philadelphia (2001)
- [10] H. Fehske, A.P. Kampf, M. Sekania and G. Wellein, Nature of the Peierls- to Mott-insulator transition in 1D. Eur. Phys. J. B **31**, 11-16 (2003)